Analysis of Charging of the HTV-4 Based on On-Orbit Data

Daisuke Tsujita, Teppei Okumura, Yuki Kobayashi, Toru Kasai, Yasushi Ohkawa,

Kiyokazu Koga, and Mengu Cho[1]

Abstract— **After three H-II Transfer Vehicles (HTVs) had finished their mission to resupply the International Space Station (ISS), NASA requested data of the HTV's potential to evaluate the charging/discharging process that occurs when the HTV docks to the ISS. In order to measure this data, a new instrument was installed on the 4th HTV. This instrument allows us to measure the HTV-4 surface potential relative to the surrounding plasma, and is called Advanced Technology On-orbit Test Instrument for space Environment-mini (ATOTIE-mini). The ATOTIE-mini observed the HTV's local potential in the orbit for more than one month. The measured potential during the HTV solo-flight phase varied between -30 to -60 V in sunlight and was about 0 V in eclipse conditions. The HTV's potential during the time when it was docked to the ISS followed the ISS's potential with an almost constant offset of about 10 V. The data measured by ATOTIE-mini are consistent with those measured by the floating potential measurement unit on the ISS, and thus are considered reliable. The HTV's potential level itself was acceptable for ISS. Note that the solar array panels can generate up to approximately 120 V, which is much larger than the absolute potential range in sunshine. We analyze the potential distribution on the HTV surface by a multi-utility spacecraft charging analysis tool, because ATOTIE-mini can only observe one point on the HTV surface. The analysis results are discussed with respect to the flight attitude.**

Keywords—HTV, Charging analysis, Ionosphere, Spacecraft charging

Nomenclature

B	Magnetic field strength.
e	Elementary charge.
F	Focus factor for current collection.
$n_{i/e}$	Ion/electron density in space.
$N_{cp/cn}$	Number of cells with positively/negatively charged electrodes.
N_p	Number of illuminated solar cell strings connected in parallel.
S_c	Conductive Area of a single solar cell.
S_r	Conductive area facing the ram region.
$T_{i/e}$	Ion/electron temperature.
T_{se}	Secondary electron temperature.
T_{pe}	Photoelectron temperature.
U_{cell}	Output voltage of a single solar cell
V_{orb}	Orbital velocity of the HTV.
$V_{thi/the}$	Ion/electron thermal velocity.
λ_D	Debye length.

I. Introduction

The International Space Station (ISS) uses a plasma contactor to maintain all surfaces within -40 V to 40 V of the surrounding plasma potential to prevent damages due to discharging or electrical shock hazards to the ISS crew [1,2]. The Floating Potential Measurement Unit (FPMU) is used to monitor the ISS's potential. Because before 9 August 2013 no visiting vehicle had carried an electrometer, there were no detailed data available regarding the charging behavior resulting from mutual interactions of huge structures such as the ISS and the H-II Transfer Vehicle (HTV) during approach and departure.

The HTV is frequently used to resupply the ISS and has been providing flight opportunities for users as an on-orbit platform from HTV-4 onwards [3]. The HTV's anti-charging design follows the ISS standard, and past operations went well. Since NASA requested data of the HTV's potential for evaluating charging/discharging processes during berthing to the ISS, an electrometer was installed on HTV-4. This electrometer successfully measured the potential and the obtained data well correspond to the data of the ISS's potential. This paper has two purposes. Firstly, the discussion of the relation between the measured on-orbit potential and the operation phases (e.g. solo-flight with different flight attitudes) of HTV-4. Secondly, the development of an analysis model, and the validation of the model by comparing the predicted results and the on-orbit data for the solo-flight phase. We hope that our discussion will contribute to the development of next-generation vehicles, such as HTV-X [4].

II. HTV

A. Overview

The HTV is a logistic supply and waste disposal vehicle for the ISS, and has been developed by the Japan Aerospace Exploration Agency (JAXA). Fig. 1 shows the configuration

of the HTV. The HTV consists of a Pressurized Logistics Carrier (PLC), an Unpressurized Logistics Carrier (ULC) including an Exposed Pallet (EP), an Avionics Module (AM), and a Propulsion Module (PM).
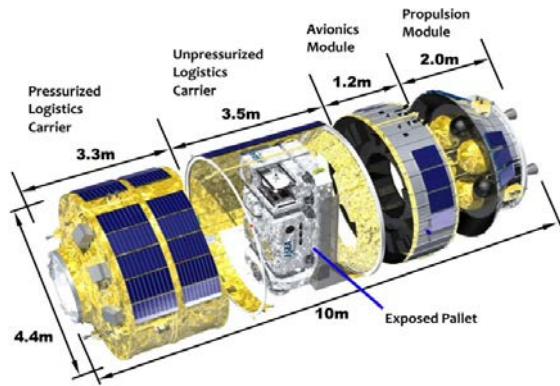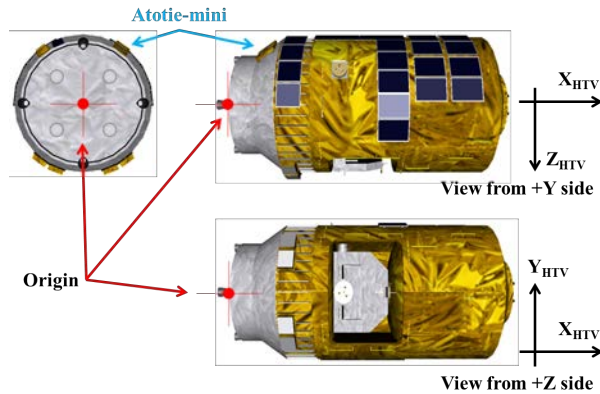

Fig. 1. HTV system configuration [3].

Fig. 2. Three different views of the HTV. The SAPs are mainly mounted on the upper side in the view from +Y.

Cargo is transported inside the PLC, and on the EP. The AM is used for navigation and control of electrical power subsystems. The PM contains the main engines for orbital maneuvers. There are 28 Reaction Control Systems (RCSs) thrusters for attitude control on several part. The fifty-five solar array panels (SAPs) are mounted on the HTV body as shown in the right upper view in Fig. 2. For thermal control, the PLC and ULC are covered by multilayer insulation (MLI). The AM is covered by silver teflon, and the PM by beta cloth. The conductive surfaces, which can collect ions or electrons from ambient plasma, are those of the thrusters, guiding parts for astronauts, and the electrodes on the SAPs.

Next, we briefly introduce the mission profile of HTV-4. HTV-4 was launched from the Tanegashima Space Center on a H-IIB launch vehicle on 3 August 2013. About 6 days later, after its automatic rendezvous, it docked to the ISS on 9 August 2013. After it had stayed at the ISS about one month, the HTV was loaded once again with unused and/or unnecessary items. It departed from the ISS on 4 September 2013. The HTV-4 finally reentered into the Earth's atmosphere to dispose those items on 7 September 2013.

As for the rendezvous, the altitude was approximately 300 to 400 km, the inclination angle was 51.6°, and the beta angle, that is the Sun's angle relative to the orbital plane, varied from -75 to +75°. The flight attitude of the HTV can be classified into Local Vertical Local Horizontal (LVLH), Yaw+90°, Yaw-90°, and the Yaw180° as shown in Fig. 3. These flight orientations are used to maximize the SAP power generation under a certain beta angle, because the SAPs which are fixed to the body, cannot track the sun. The EP always faces Earth during the solo-flight phase.
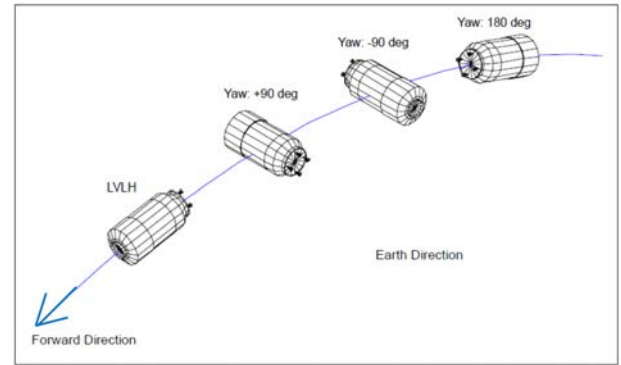

Fig. 3. HTV attitude definition in the solo-flight phase.

B. Electrometer

The electrometer designed for this mission is also called Advanced Technology On-orbit Test Instrument for space Environment-mini (ATOTIE-mini). It was installed by exchanging one of the SAPs on the PM with ATOTIE-mini, as shown in Fig. 4. Fig. 5 shows an illustration of ATOTIE-mini (upper panel) and a photograph. The controller of ATOTIE-mini was mounted on a seat, which was covered by MLI on the side facing space. In addition, silver teflon covered the top side of the controller to efficiently radiate heat. In the ionospheric plasma environment, the relative surface potential of a dielectric material, such as MLI, is lower by a few times the energy of electrons in the range from 0.1 eV to 0.3 eV. No conductive parts were exposed to the ambient plasma, and thus any interference with the potential measurement was avoided.

The ATOTIE-mini was equipped with a passive and an active sensor. A Surface Charging Monitor (SCM) [6,7,8], which is a high-impedance plasma probe with a lot of flight experience on sounding rockets, scientific satellites, etc., was used as passive sensor. We note that the SCM cannot make reliable measurements in the low-density wake region. The employed active sensor, called TREK-3G, is a device that adjusts the probe's surface potential to the value of the surrounding plasma and then reads the probe potential. It has a higher accuracy than the SCM but at the time of the HTV-4 mission had been used only once (on Horyu-2) [9]. Therefore, a system like SCM was required as back up. Section IV deals with the TREK-3G data. The details of this sensor including the measurement mechanism have been described by Okumura et al. [10]. Both sensors measured the potential of the ambient plasma with respect to that of the HTV in the range from -200 to +200 V. The sampling rate was 0.1 Hz.
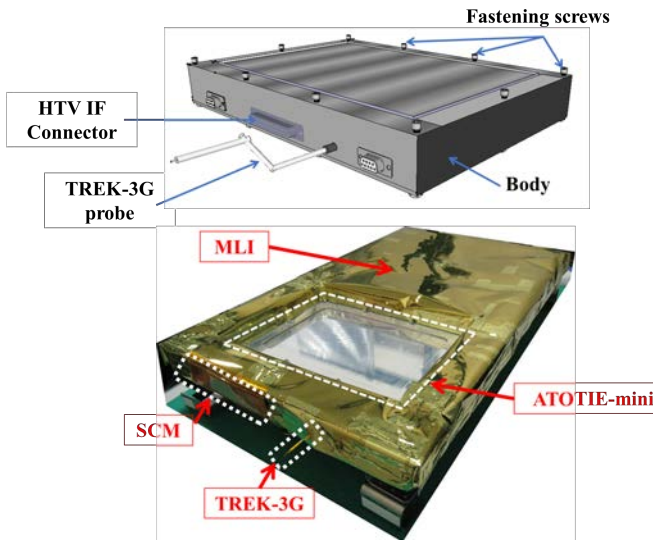
Fig. 4. ATOTIE-mini on the HTV-4 in orbit.

Fig. 5. Illustration of ATOTIE-mini and photograph of the device in the mounting seat.

III. Measurement results by ATOTIE-mini

A. Data averaging

Before we discuss the relation between the on-orbit data measured by ATOTIE-mini and the different operation phases of HTV-4, we explain how we averaged the raw on-orbit data. To verify that the averaging results in physically meaningful values, we compared the TREK-3G raw data and the FPMU data obtained during the time when HTV-4 was docked to the ISS. In this mission phase, the HTV is grounded to the ISS through the common berthing mechanism. The FPMU has been described in [7], [8] and [11]. The on-orbit data of ATOTIE-mini and the FPMU are shown in the upper panel of Fig. 6. The FPMU potential data shown here includes the potential difference that is induced by the different Lorentz

force at the position of ATOTIE-mini. The lower graph of Fig. 6 compares the SCM and FPMU data. The raw data of TREK-3G and SCM exhibit fluctuations because the design was not optimized to suppress radio emission noise inside the controller. The effect of the radio emission on the measurement data is periodic. Therefore, we are able to eliminate the noise by applying a moving average with a period of fifty points (shown with the black solid curves). The difference between the averaged TREK-3G data and the FPMU data lies almost constant at 10 V. Therefore, we believe that the TREK-3G data is sufficiently reliable for the present purpose.

B. Summary of TREK-3G results

During the solo-flight phase, the attitude of HTV was controlled by the RCS thrusters as mentioned in Section II.A. It is well known that the current collection by the electrodes on the SAPs and the conductive parts of the spacecraft body are the major factors that determine the potential of a spacecraft in the ionospheric plasma environment [12]. The conductive area facing the ram region changes with the attitude as shown in Fig. 3. The top panels of Fig. 7, 8 and 9 show the TREK-3G measurement results for LVLH, Yaw 90° and Yaw 180°, respectively. These figures also contain the information on the total current generated by the SAPs (center panel) and the HTV-4 position in orbit (bottom panel). The total current output from the 55 SAPs clarifies the time when HTV-4 was exposed to sunshine. This current, along with the number of solar cells in series connection (35), the beta angle, and the temperature of the SAPs can be used to estimate the generated voltage. When in sunlight, the HTV's potential depends on the attitude, because of two major reasons. Firstly, the conductive area on the ram side changes with the attitude, because the potential of the HTV is mainly determined by the ion current flow from the ram side. Secondly, the sunlight's incident angle on the SAPs changes with HTV orientation. Since the output voltage of the SAPs changes with the incident angle, the potential of the HTV changes with the attitude.

Table I provides the most extreme potentials observed by TREK-3G in sunlight (day) and eclipse (night) conditions for three attitudes. The values given are the extrema of the moving averages. The minimum potential was observed for Yaw 90° (-54 V), implying that the conductive area facing the ram region was minimized in the case of Yaw 90°. This interpretation is verified in the next section. During night, the HTV was positively charged in the cases of Yaw 180° and Yaw 90°. The positive charging can be reproduced by the multi-utility charging analysis tool (MUSCAT) [13,14].

In Fig. 10 we show the results obtained during the operation of the space station robot manipulator system (SSRMS). During SSRMS operation, the power control unit of HTV-4 was switched off and the HTV was electrically connected to the ISS with a resistance of 5 kΩ. Therefore, the potential of the HTV cannot be same as the potential of the ISS. Additionally, the potential difference between the positive and negative electrodes on the SAPs was open-circuit voltage. By using the number of series-connected solar cells, we have predicted a possible range of 70 to 120 V for the open-circuit voltage [10]. This suggests a more negative HTV potential during SSRMS operation compared to that of the solo-flight phase. However, the extreme potential during SSRMS

operation (-50V) is comparable to that during solo-flight phase (-54 V for Yaw 90°). The theoretical calculation of the HTV potential during SSRMS operation is discussed in [10].

TABLE I.   SUMMARY OF AVERAGED POTENTIAL EXTREMA DURING SOLO-FLIGHT PHASE CALCUATED FROM THE RAW DATA SETS INDICATED IN FIGS. 7, 8 AND 9

No	Attitude	beta[deg]	height[km]	Day[V]	Night[V]
1	LVLH	68.6	301	-39	-7
2	Yaw90	66.2	288	-54	+2
3	Yaw180	60.1	406	-49	+6

IV.   CHARGING ANALYSIS

A. Overview

Besides discussing the on-orbit data, we also need to confirm the validity of the charging model for the HTV. Therefore, we discuss two kinds of charging models in this section. In Section IV.B we introduce a numerical calculation that is based on a simple expression for the current collection. The more complex simulation model discussed in Section IV.C is based on MUSCAT.

In order to evaluate the charging model of the HTV, we analyze each attitude during the solo-flight phase. The overview of the employed conditions are shown in Table II. Since HTV-4's flight attitude was mainly LVLH, the beta angle was varied. In case of LVLH, the potential with the highest beta is selected as the case study, because the SAPs generate maximum power.

TABLE II.   CONDITIONS CONSIDERED IN THE PRESENT ANALYSIS

No	Attitude	beta[deg]	height[km]	Plot
1	LVLH	68.6	301	Fig.7
2	Yaw180	60.1	406	Fig.8
3	Yaw90	66.2	288	Fig.9

B. Numerical analysis

The potential derived in this model is that at which the ion and electron currents collected by both the exposed conductive surfaces and the electrodes on the SAPs are balanced. The photoelectron current is negligible, because its current density is small compared to the current density of ionospheric electrons [15]. Because HTV-4 did not pass through the auroral oval, we do not consider auroral electrons for the analysis of the HTV charging. Accordingly, we define the ion current collected by exposed conductive surfaces on the ram side (I_s), the ion current collected by negative electrodes on the SAPs (I_{an}), and the electron current collected by the positive electrodes (I_{ap}) as shown in (1) to (3), respectively.

$$I_s = e·n_i·V_{orb}·S_r . \qquad (1)$$

$$I_{an} = U_{cell}·N_p·N_{cn}·(1/4) ·e·n_i·V_{thi}·S_c·F. \qquad (2)$$

$$I_{ap} = U_{cell}·N_p·N_{cp}·(1/4) ·e·n_e·V_{the}·S_c·F. \qquad (3)$$

Here, S_r is the conductive surface area facing the ram region, and thus depends on the attitude. N_{cn} is the number of solar cells that attract ions on a single solar cell string consisting of 35 solar cells connected in series. N_{cp} is the number of solar cells that attract electrons on a single solar cell string. Hence, the sum of N_{cn} and N_{cp} is constant:

$$N_{cn} + N_{cp} = 35. \qquad (4)$$

The total number of solar cell strings connected in parallel, is 285 (that is, each SAP contains approximately 5 strings, depending on panel size). N_p is the number of solar cell strings exposed to sunlight. The beta angle and attitude of the HTV allow us to estimate N_p. U_{cell} is the voltage generated by a single solar cell, and it varies from 2.0 to 3.1 V depending on the surface temperature. We used plasma parameters that are typical for the HTV's orbital environment: $n_{e,i} = 10^{12}\,m^{-3}$, V_{orb} = 8 km/s, T_e and T_i are 0.1 and 0.5 eV, respectively. We use a so-called focus factor F to account for the enhancement of current collection due to the sheath. Hastings et al. [12] employed computer simulations to explore the enhancement of the plasma current due to exposed high-potential surfaces such as interconnect and bus bars of solar cell arrays. While this enhancement depends on the potential, preliminary calculations suggested that a constant value of F = 10 should be adequate for our purpose. The potential of the HTV can be obtained from the following condition:

$$I_s + I_{an} + I_{ap} = 0. \qquad (5)$$

The S_r, N_p, and the calculated HTV potential are summarized in Table III together with the experimental on-orbit data. The evaluated N_{cn} and N_{cp} values allow us to predict the fraction of the generated voltage that is positive with respect to the plasma. From Table III, we find that the predictions for LVLH and Yaw 90° well agree with the on-orbit data. On the other hand, the predicted potential for Yaw 180° is too high. To explain this overestimation, we have to consider that for this attitude, the main engines face the ram region. The entire surface area of the main engines is included in S_r in the above calculation. Because the local wake structure caused by the nozzle is not considered, this approximation results in an ion current that is higher than the actual value. Therefore, the calculated potential is higher than the experimentally measured value. The most negative potential occurs for Yaw 90°. Since the S_r in the case of Yaw 90° is smaller than that of the other attitudes, the amount of ion current should be smaller. Therefore, the most negative potential was experimentally observed for Yaw 90°. As such, even this simple numerical model allows us to understand some important features of the HTV charging.

TABLE III.   SUMMARY OF THE SIMPLE NUMERICAL ANALYSIS

Attitude	LVLH	Yaw 90°	Yaw 180°
S_r [m2]	3.5	2.3	6.1
N_p	176	266	171
N_{cn}, N_{cp}	3520, 2640	6650, 2660	2736, 3249

On-orbit data [V]	-39	-54	-49
Calculated potential [V]	-38	-57	-32

C. Simulation analysis

The simulation of the HTV charging is performed using the software MUSCAT, which was developed by JAXA [13,14]. Muranaka et al. have provided a detailed description of the simulation technique of MUSCAT [13].

MUSCAT uses the particle-in-cell (PIC) and the particle-tracking (PT) schemes and has a grid consisting of 128×128×128 cells. In the present simulation, the potential of the boundaries of the computational space are fixed at 0 V. In order to simulate the entire body of the HTV in the simulation space, we set the cell size to 30 cm cubed. As shown in Fig. 11, the model of the HTV is located at the center of the computational grid. Because the size of the HTV is 4.4 m in diameter and 10 m in length, the model of the HTV extends 15 cells in both Y and Z directions and 34 cells in X direction. Because of the limited grid resolution, several parts such as the main engine thrusters and RCS thrusters, cannot be resolved in the grid system. However, the electrical properties are included in the grid system. The ATOTIE-mini is represented by a combination of conductive cells (blue) and insulating cells (red). The HTV surface consists of about 200 different materials. Smaller surfaces, such as handrails for the crew are ignored. The small high-potential surfaces on the SAPs are grouped and represented by separate surfaces of approximately the same total surface area.

Because the cell size is too large compared to the Debye length λ_D, the sheath structure around the HTV body cannot be simulated in the present model. Therefore, we use a potential-independent focus factor F to account for the enhancement of the plasma current from the sheath. Except where otherwise stated, we use $F = 10$, because this value provides the most accurate results for Yaw 90°. In addition, we employ 2.0 and 1.5 eV for T_{se} and T_{pe}, respectively. In the considered environment λ_D is ≈ 0.3 cm, the Larmor radius is ≈ 3 cm, and the sheath depth is approximately 30 cm. Since these values are smaller than the cell size, the motion related to the magnetic field B cannot represented in the simulation. Hence, the simulation is for $B = 0$ T. For the other simulation parameters we use those of the numerical analysis.
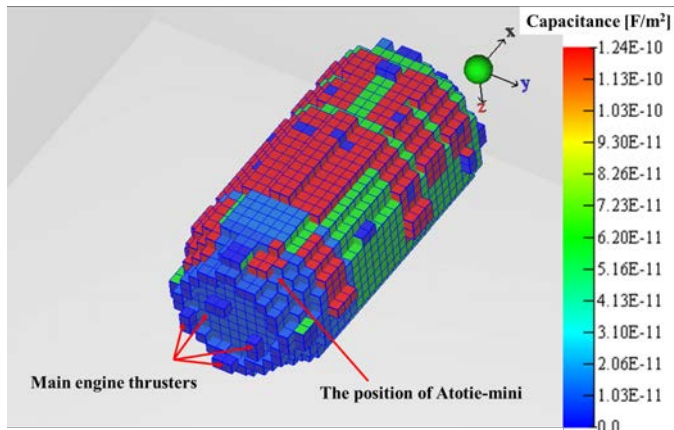
Fig. 11. Grid model of the HTV.

The results of the simulations for sunlight and eclipse conditions are summarized in Table IV. The simulation result for the case of night well corresponds to the on-orbit data. On the other hand, the simulation result for the case of day exhibits a large difference relative to the on-orbit data. We interpret the simulation results in Section IV.D.

Fig. 12 and 13 show the calculated potential of ATOTIE-mini at day and night, respectively. The graphs compare the potential of the conductive HTV body (orange curves) and the surface potential at the location of ATOTIE-mini (blue curves). The number of iteration steps in the simulation is 4000 for night, and 8000 for day. The time scale is 1×10^{-8} s/step. The number of iterations is considered adequate because both potentials have converged to stable levels at the end of the simulation.

Fig. 14 and 15 show two views of the surface potential distribution of the HTV in sunlight. Both figures represent the calculation results at the final iteration step. The potential of the exposed conductive surfaces equals the body potential, which corresponds to blue in terms of the color bar. The potential of the dielectric parts reaches equilibrium, that is, the same potential as that of the ambient plasma. The surface potential of the dielectric parts is discussed in [5]. In the cases of Yaw 180° and LVLH, it was not possible to obtain a surface potential at equilibrium with the ambient plasma even when using different values for F. The potential distribution in case of LVLH is shown in Fig. 16. Here, a part of the dielectric surface has a positive potential relative to the ambient plasma. In addition, the body potential has not converged within 8000 iteration steps as shown in Fig. 17. The reason for this result is discussed in Section IV.D.

TABLE IV. COMPARISON BETWEEN THE HTV'S POTENTIAL OBTAINED FROM THE ON-ORBIT DATA AND THE SIMULATION. NOTE THAT THE ON-ORBIT DATA IS SAME AS THE DATA SHOWN IN TABLE I

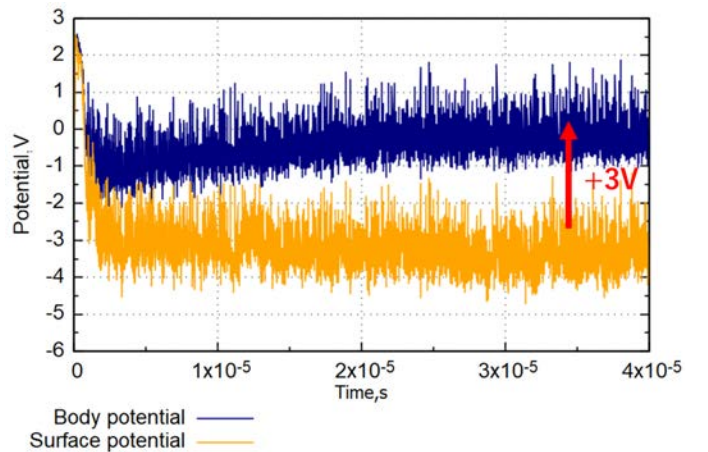| No	Yaw90°	Simulation	On-orbit data
1	Day	-42 V	-54 V
2	Night	+4 V	+2 V

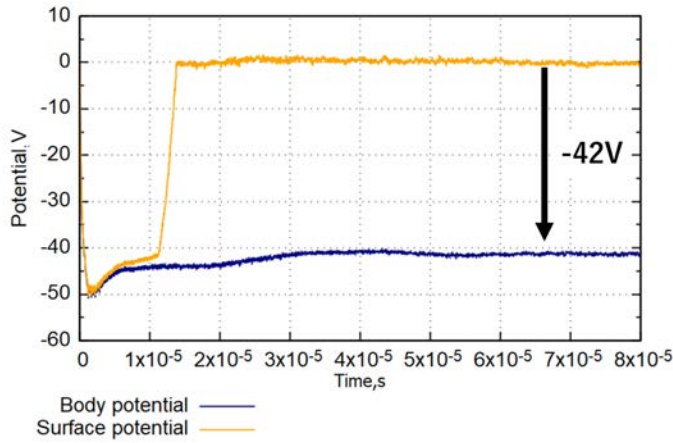Fig. 12. Calculated ATOTIE-mini potential at night for Yaw 90°.

Fig. 13. Calculated ATOTIE-mini potential at day for Yaw 90°.

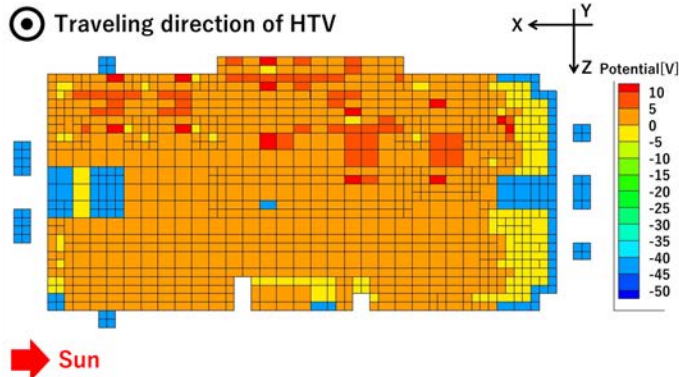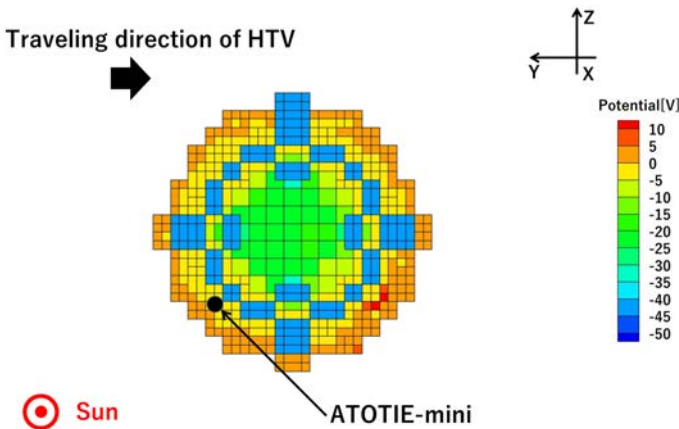Fig. 14. X–Z plane view of the potential distribution for Yaw 90°.

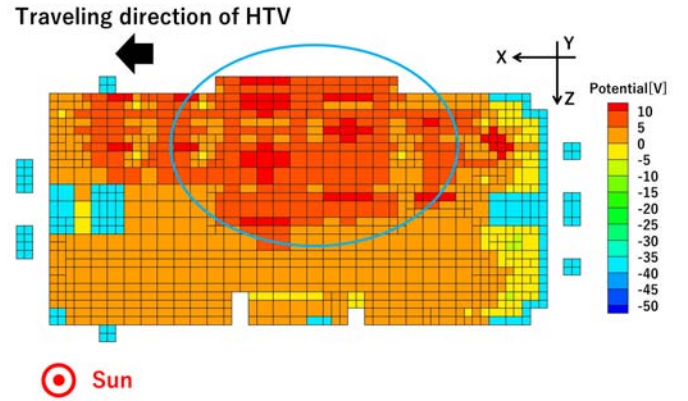Fig. 15. Y–Z plane view of the potential distribution for Yaw 90°.

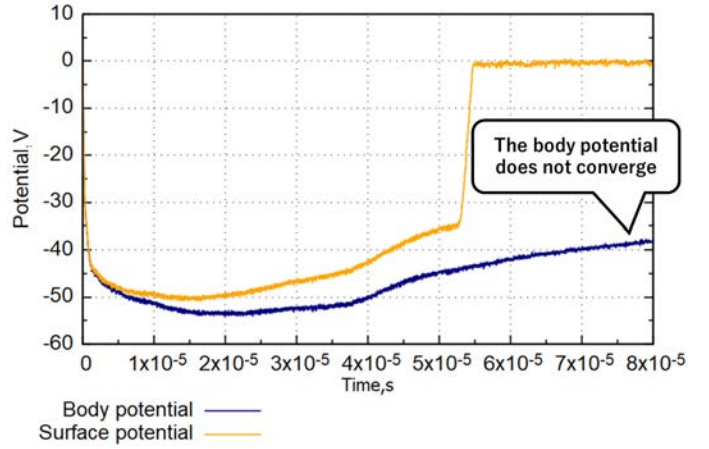Fig. 16. X–Z plane view of the potential distribution for LVLH.

Fig. 17. Calculated ATOTIE-mini potential at day for LVLH.

D. Discussion

Firstly, we explain why the body potential differs from the SAP's electrode voltage. As mentioned in Section III.B, the estimated maximum for the generated voltage is 120 V. This means that the lowest possible potential of the HTV should be near -120 V. Both numerical analysis and simulation matched on-orbit data, showing that the potential of the HTV is mitigated because of the ion current that strikes the conductive part facing the ram region. In addition, the potential of a spacecraft changes with attitude as has been reported in other on-orbit measurements [17]. The theoretical analysis explains that the HTV body potential rises above the electrode potential due to collection of ions by the exposed conductive areas.

Secondly, we investigate why the simulation result can only explain the on-orbit data for Yaw 90°. We note that the HTV area facing the ram region under Yaw 90° contains many SAPs and thus exposes a smaller conductive area. Therefore, the simulation can adequately reproduce the sheath effect even with a constant focus factor. On the other hand, the ram-facing HTV surface under LVLH and Yaw 180° has almost no SAPs. Therefore, the simulation requires a F of nearly 40 for the electrons that are collected by the electrodes on the SAPs. However, the effect of the ion current is more dominant under LVLH and Yaw 180°, and thus the time step has to be adjusted to obtain the correct result. Note that the simulation in Fig. 17 cannot converge due to its limited number of iteration steps. To accurately predict the HTV charging under various

conditions, we need to increase the total number of cells of the grid and the temporal computation domain by rewriting the simulation code.

V. SUMMARY AND FUTURE WORK

We analyzed the HTV-4 potential data measured in orbit by ATOTIE-mini. By comparing the data with the FPMU data from the ISS, it was confirmed that TREK-3G provides valid data. We then discussed the results of potential measurements during solo-flight phase and SSRMS operation. The data shows that the potential of the HTV during solo-flight phase changes with the attitude of HTV-4. In particular, we confirmed that the most negative potential occurs under Yaw 90°. The dependence of the potential on the HTV attitude was analyzed by using both a simple numerical analysis and the simulation software MUSCAT. The numerical analysis reveals that the potential of HTV-4 in sunlight is a result of current collection via the SAPs and conductive parts on the HTV. The simulation technique still needs further improvements in terms of grid resolution and temporal computation domain. However, we successfully simulated the potential of HTV-4 for Yaw 90°, where a potential-independent focus factor can be used.

Through the on-orbit measurements and the results of the numerical analysis, the following HTV-charging mechanisms were clarified:

1) The ion current collected by the exposed conductive areas reduces the extent of (negative) charging with respect to ambient plasma.
2) When the HTV surface facing the ram region has a large exposed conductive area and only few SAPs, the HTV body potential is mainly determined by the ion current.

Although the numerical analysis allowed us to calculate the potential of the HTV in sunlight, we used some assumptions such as the constant focus factor. In future, we need to improve our simulation tool to simulate the potential of a large spacecraft under a dense plasma environment including effects of the sheath. Such a simulation tool is useful for the development of next generation vehicles such as HTV-X.

ACKNOWLEDGMENT

REFERENCES

[1] S. Koontz, M. Valentine, T. Keeping, M. Edeen, W. Spetech and P. Dalton, "Assessment and control of spacecraft charging risks on the International Space Station." 8th Spacecraft Charging Technology Conference, Huntsville, AL, 2003, NASA/CP-2004-213091.

[2] A. Hernandez-Pellerano et al., "International Space Station (ISS) Plasma Contactor Unit (PCU) Utilization Plan Assessment Update." Report/Patent Number: NASA/TM-2014-218512.

[3] D. Tsujita, T. Kasai, H. Uematsu, M. Harada, T. Fukatsu and H. Sasaki, "Experiments Plan on the HTV." Trans JSASS Aerospace Tech. Japan, Vol. 12, No. ists29, pp.Tg_1-Tg_4. 2014. DOI:10.2322/tastj.12.Tg_1.

[4] D.Tsujita., T.Nakamura., K.Shibata., S.Matsuo., T.Wakatsuki., Y.Kondoh., K.Nagahama., T.Uchiyama., N.Ito., "HTV-X system integration plan." Proceedings of the International Astronautical Congress, IAC, Volume 15, 2017, Pages 9887-9891.

[5] Cho, M., and Hastings, D. E., "Dielectric Charging Process and Arcing Rates of High Voltage Solar Array," Journal of Spacecraft and Rockets, Vol. 28, No. 6, 1991, pp. 698-706. doi:10.2514/3.26302

[6] K. Koga and H. Matsumoto, "Measurement results of the plasma monitor of onboard Space Environment Data Acquisition equipment - Attached Payload (SEDA-AP)." 12th Spacecraft Charging Technology Conference, Albuquerque, NM, USA.

[7] Ferguson, D. C., "FPP Results-Final Report," IEEE Transaction on Plasma Science, Vol. 37, No. 2, 2009, pp. 369-374.doi:10.1109/TPS.2008.918667

[8] Minow, J. I., Wright, K. H., Jr., Chandler, H. O., Coffey, V. N., Craven, P. D., Schneider, T. A., Parker, L. N., Ferguson, D. C.,Koontz, S. L., and Alred, J. W., "Summary of 2006 to 2010 FPMU Measurements of International Space Station Frame PotentialVariations," 11th Spacecraft Charging Technology Conference, Repts. M10-0761, M10-1084, NASA Marshall Space Flight Center, Huntsville, AL, Sept. 2010.

[9] A. Takahashi, A. R. Khan, H. Masui, M. Iwata, K. Toyoda and M. Cho, "Preliminary Report on On-orbit Experiment on High Voltage Technology Demonstration Satellite, HORYU-II." 63rd International Astronautical Congress, IAC-12-D5.3.13, Naples, Italy, 2012.

[10] T.Okumura., Y.Ohkawa., K.Koga., S.Kawakita., S.Kawamoto., Y.Kobayashi., T.Kasai., "Charging of the H-II Transfer Vehicle at Rendezvous and Docking Phase", Journal of Spacecraft and Rockets, Vol. 55, No. 4 (2018), pp. 971-983. DOI: 10.2514/1.A34068

[11] Wright, K. H., Jr., Swenson, C. M., Thompson, D. C., Barjatya, A., Koonts, S. L., Schneider, T. A., Vaughn, J. A., Minow, J. I., Craven, P. D., Coffey, V. N., Parker, L. N., and Bui, T. H., "Charging of the International Space Station as Observed by the Floating Potential Measurement Unit: Initial Results," IEEE Transaction on Plasma Science, Vol. 36, No. 5, 2008, pp. 2280-2293. doi:10.1109/TPS.2008.2003257

[12] Hastings, D. E., Cho, M., and Wang, J., "Space Station Freedom Structure Floating Potential and the Probability of Arcing," Journal of Spacecraft and Rockets, Vol. 29, No. 6, 1992, pp. 830-834. doi:10.2514/3.25538

[13] Muranaka, T., Hosoda, S., Kim, J.-H., Hatta, S., Ikeda, K., Hamanaga, T., Cho, M. Usui, H., Ueda, H.O., Koga, K., Goka, T. Development of multi-utility spacecraft charging analysis tool (MUSCAT), IEEE Transactions on Plasma Science, Volume 36, Issue 5 PART 2, 2008, Pages 2336-2349. DOI: 10.1109/TPS.2008.2003974

[14] S. Hatta et al., "Accomplishment of Multi-Utility Spacecraft Charging Analysis Tool (MUSCAT) and its future evolution," Acta Astronautica, 64, 2009, pp.495-500. DOI:10.1016/j.actaastro.2008.07.023

[15] Hastings, D., and Garrett, H., Spacecraft Environment Interactions, Cambridge Univ. Press, New York, 1996, pp. 146-148.

[16] Klimov, S. I., Lissakov, V. Y., Lapshinova, V. O., Mashkov, A. S., Mednikov, A. B., Pushkin, M. N., and Antropov, N. N., "In Flight Measurement of the Outside Surface Potential of the 'MIR' Orbital Station," Proceedings of the 7th International Conference, European Space Agency, Noordwijk, The Netherlands, 2001.

[17] Klimov, S. I., Lissakov, V. Y., Lapshinova, V. O., Mashkov, A. S., Mednikov, A. B., Pushkin, M. N., and Antropov, N. N., "In Flight Measurement of the Outside Surface Potential of the 'MIR' Orbital Station," Proceedings of the 7th International Conference, European Space Agency, Noordwijk, The Netherlands, 2001.

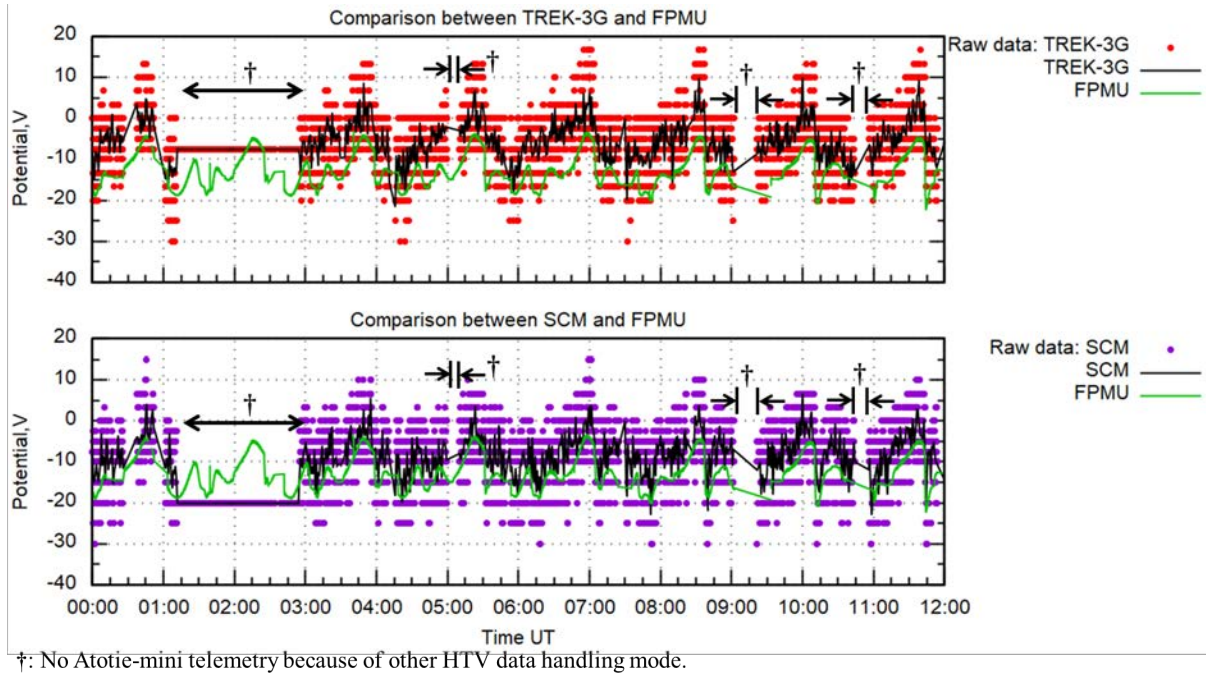†: No Atotie-mini telemetry because of other HTV data handling mode.

Fig. 6. Potential measurement during the time when HTV-4 was attached to the ISS.
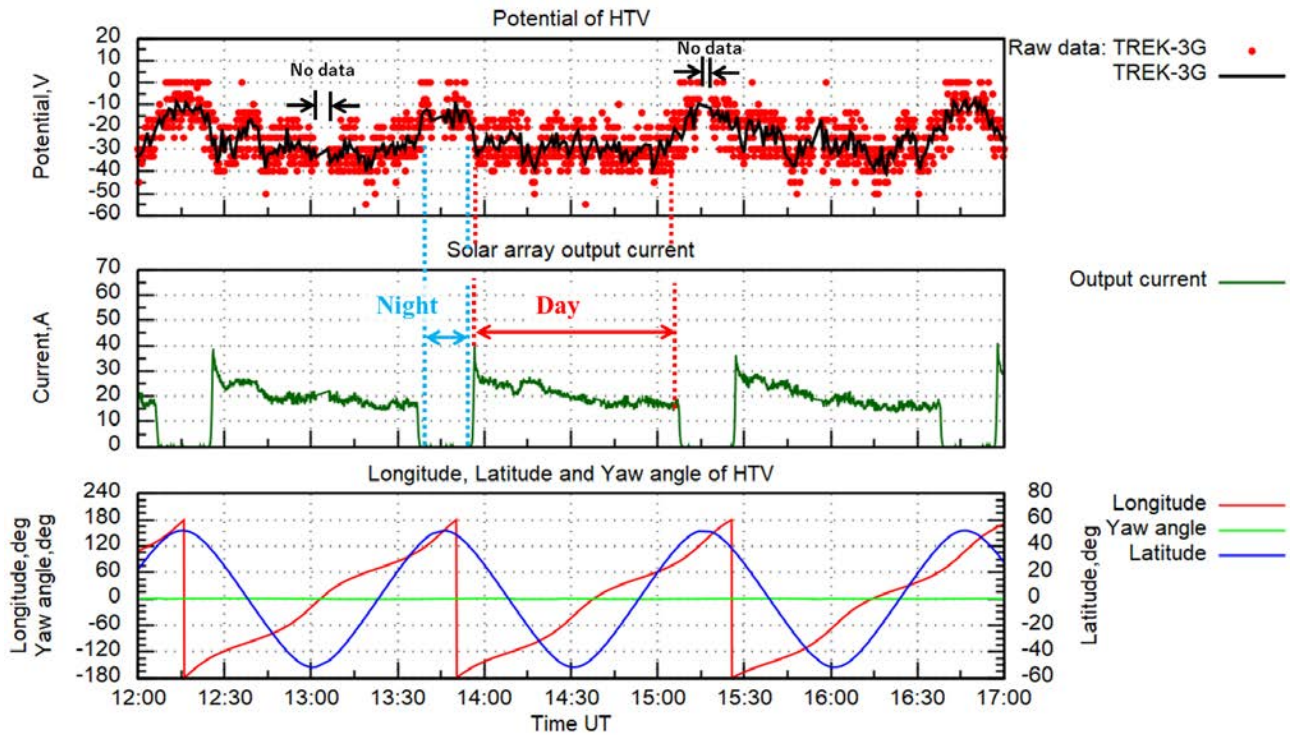

Fig. 7. Potential of HTV-4 (top panel), total output current of the SAPs (center panel), and HTV position (bottom panel) in case of LVLH.
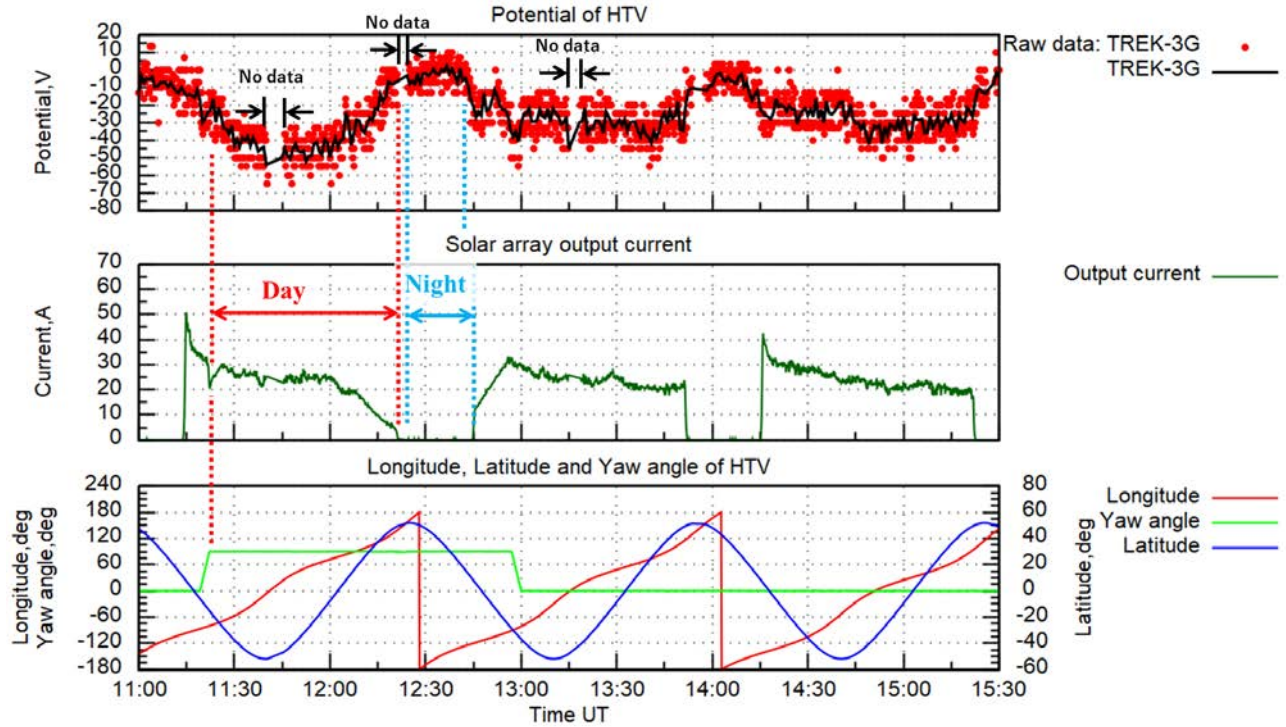
Fig. 8. Potential of HTV-4 (top panel), total output current of the SAPs (center panel), and HTV position (bottom panel) in case of Yaw 90°.
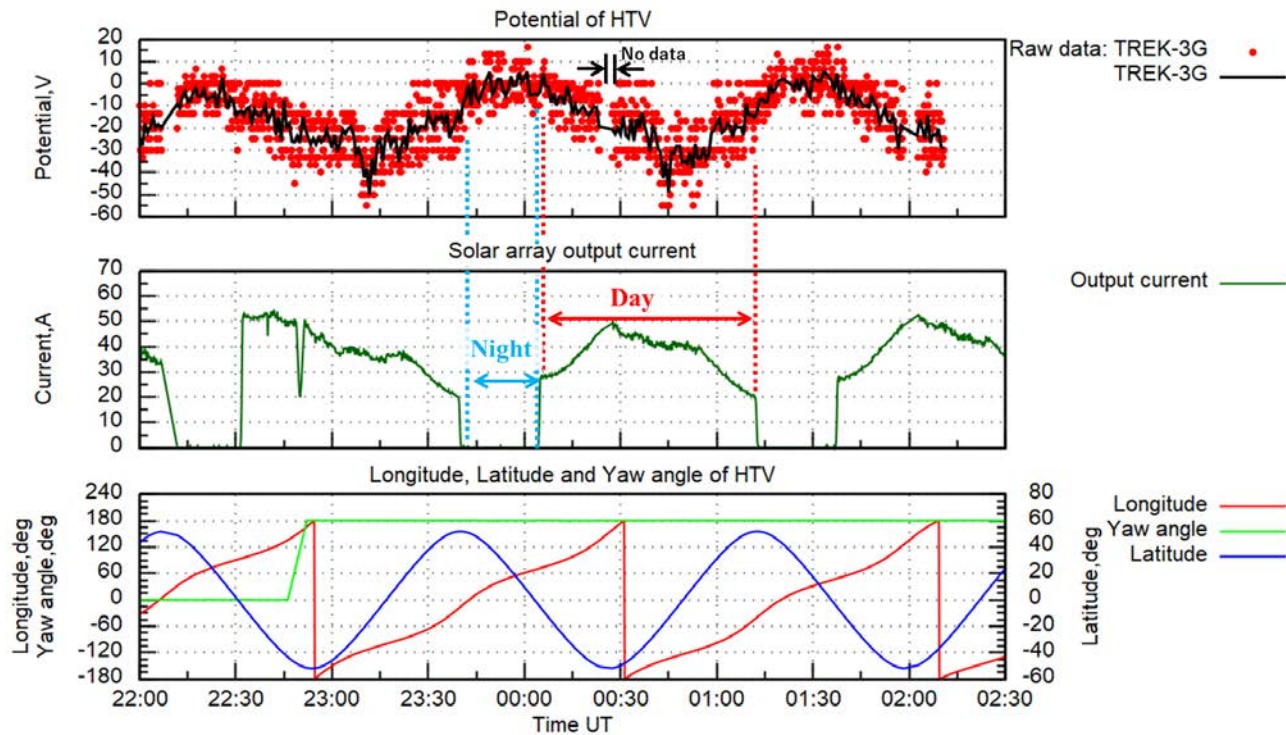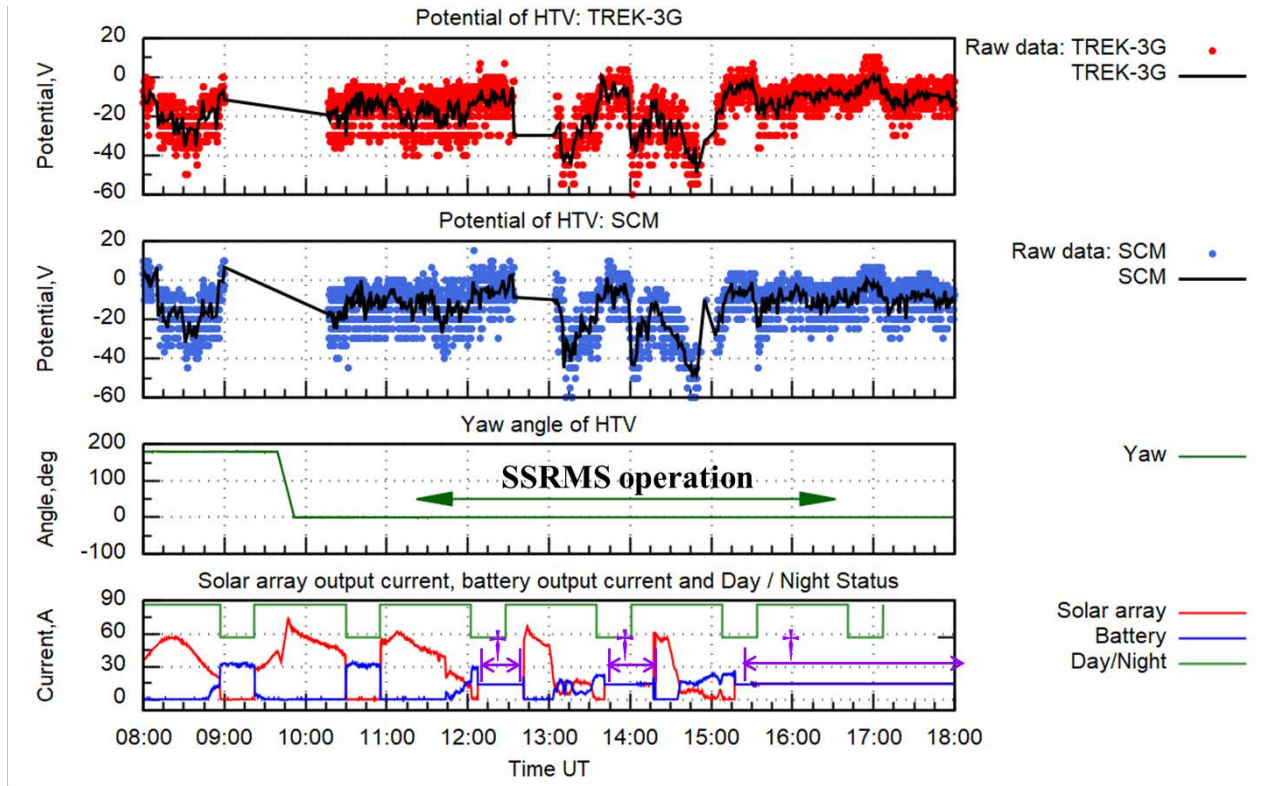

Fig. 9. Potential of HTV-4 (top panel), total output current of the SAPs (center panel), and HTV position (bottom panel) in case of Yaw 180°.

†: The solar array circuits are disconnected from the power control unit of HTV.

Fig. 10. The potential of HTV-4 measured by TREK-3G and SCM (upper two panels) and related data obtained during SSRMS operation.